Electrochemical Growth and Characterization of Polyoxometalate-Containing Monolayers and Multilayers on Alkanethiol Monolayers Self-Assembled on Gold Electrodes

Long Cheng, Li Niu, Jian Gong,† and Shaojun Dong*

Laboratory of Electroanalytical Chemistry, Changchun Institute of Applied Chemistry, Chinese Academy of Sciences, Changchun, Jilin 130022, People's Republic of China

Received September 3, 1998. Revised Manuscript Received March 15, 1999

A general strategy has been developed for fabrication of ultrathin monolayer and multilayer composite films composed of nearly all kinds of polyoxometalates (POMs), including isopolyanions (IPAs), and heteropolyanions (HPAs). It involves stepwise adsorption between the anionic POMs and a cationic polymer on alkanethiol (cysteamine and 3-mercaptopropionic acid) self-assembled monolayers (SAMs) based on electrostatic interaction. Here a Keggin-type HPA $SiMo_{11}VO_{40}^{5-}$ was chosen as a main representative to elucidate, in detail, the fabrication and characterization of the as-prepared composite films. A novel electrochemical growth method we developed for film formation involves cyclic potential sweeps over a suitable potential range in modifier solutions. It was comparatively studied with a commonly used method of immersion growth, i.e., alternately dipping a substrate into modifier solutions. Growth processes and structural characteristics of the composite films are characterized in detail by cyclic voltammetry, UV−vis spectroscopy (UV−vis), X-ray photoelectron spectroscopy (XPS), micro-Fourier transform infrared reflection−absorption spectroscopy (FTIR-RA), and electrochemical quartz crystal microbalance (EQCM). The electrochemical growth is proven to be more advantageous than the immersion growth. The composite films exhibit well-defined surface waves characteristic of the HPAs' redox reactions. In addition, the composite films by the electrochemical growth show a uniform structure and an excellent stability. Ion motions accompanying the redox processes of $SiMo_{11}VO_{40}^{5-}$ in multilayer films are examined by in situ time-resolved EQCM and some results are first reported. The strategy used here has been successfully popularized to IPAs as well as other HPAs no matter what structure and composition they have.

1. Introduction

Polyoxometalates are a distinctive class of inorganic metal−oxygen cluster compounds which are unique in their topological and electronic versatility. They have been found applications in fields as diverse as catalysis, analysis, medicine, biochemistry, material science, and so on.[1] Among the large family of POMs, some IPAs and HPAs with Keggin or Dawson structures have the ability to proceed in multiple, consecutive, and reversible multielectron reductions without decomposition to mixed-valence species (called heteropolyblues (HPBs) for HPAs). The IPAs and HPAs have long-term chemical stability with good ionic and electronic conductivity, which are useful and attractive in modification of electrode surfaces. Attaching redox-active POMs onto electrodes simplifies their electrochemical studies and facilitates their applications in many fields. A number of strategies have been developed to prepare chemically modified electrodes (CMEs) with a variety of IPAs and HPAs, such as (i) electrodeposition at a sufficiently negative potential;[2a−e] (ii) adsorbtion on electrode surfaces;[3a−c,4a−c] (iii) doping in conducting

* To whom correspondence should be addressed. Telephone: +86-431-5682801 ext. 5562. Fax: +86-431-5689711. E-mail: dongsj@ns.ciac.jl.cn.

† Department of Chemistry, Northeast Normal University, Changchun, Jilin 130024, People's Republic of China.

(1) (a) Pope, M. T. *Heteropoly and isopoly oxometalates*; Springer-Verlag: New York, 1983. (b) Pope, M. T.; Müller, A. *Angew. Chem., Int. Ed. Engl.* **1991**, *30*, 34.

(2) (a) Keita, B.; Nadjo, L. *J. Electroanal. Chem.* **1988**, *243*, 87. (b) Keita, B.; Nadjo, L.; Krier, G.; Muller, J. F. *J. Electroanal. Chem.* **1987**, *223*, 287. (c) Keita, B.; Nadjo, L. *J. Electroanal. Chem.* **1988**, *247*, 157. (d) Keita, B.; Nadjo, L. *J. Electroanal. Chem.* **1985**, *191*, 441. (e) Keita, B.; Bouaziz, D.; Nadjo, L.; Deronzier, A. *J. Electroanal. Chem.* **1990**, *279*, 187 and references therein. (f) Keita, B.; Bouaziz, D.; Nadjo, L. *J. Electroanal. Chem.* **1988**, *255*, 303. (g) Keita, B.; Bouaziz, D.; Nadjo, L.; Deronzier, A. *J. Electroanal. Chem.* **1990**, *279*, 187. (h) Keita, B.; Essaadi, K.; Nadjo, L. *J. Electroanal. Chem.* **1989**, *259*, 127. (i) Keita, B.; Bouaziz, D.; Nadjo, L. *J. Electroanal. Chem.* **1990**, *284*, 431. (j) Keita, B.; Dellero, N.; Nadjo, L. *J. Electroanal. Chem.* **1991**, *302*, 47. (k) Keita, B.; Belhouari, A.; Nadjo, L. *J. Electroanal. Chem.* **1993**, *355*, 235.

(3) (a) Dong, S.; Jin, Z. *J. Chem. Soc., Chem. Commun.* **1987**, 1871. (b) Dong. S.; Wang, B. *Electrochim. Acta* **1992**, *37*, 11. (c) Wang, B.; Dong, S. *J. Electroanal. Chem.* **1992**, *328*, 245. (d) Wang, B.; Dong, S. *Electrochim. Acta* **1993**, *38*, 1029. (e) Dong, S.; Jin, W. *J. Electroanal. Chem.* **1993**, *354*, 87. (f) Dong. S.; Liu, M. *J. Electroanal. Chem.* **1994**, *372*, 95. (g) Liu, M.; Dong, S. *Electrochim. Acta* **1995**, *40*, 197. (h) Dong, S.; Cheng, L.; Zhang, X. *Electrochim. Acta* **1998**, *43*, 563. (i) Dong, S.; Song, F.; Wang, B.; Liu, B. *Electroanalysis* **1992**, *4*, 643. (j) Cheng, L.; Zhang, X.; Xi, X.; Liu, B.; Dong, S. *J. Electroanal. Chem.* **1996**, *407*, 97.

10.1021/cm9806127 CCC: $18.00 © 1999 American Chemical Society
Published on Web 05/07/1999

polymers,[2f−g,3d−h,4d,5a−d] nonconducting polymers[2h−i,3i] and other polymer matrixes;[6] and (iv) other strategies.[2j−k,7,8] However, the modification strategies now available are not of sufficient quality to meet various needs. It is necessary, but challenging to explore a novel strategy for fabricating ultrathin, dense, stable, and multifunctional films with POMs on electrode surfaces.

Indeed, the self-assembly technique has been used to form organized, surface-confined monolayers or multilayers that do not possess ill-defined or nonreproducible morphological characteristics.[9,10] Among several different approaches to prepare well-defined multilayers,[11a−f] a method based on the electrostatic interaction between oppositely charged species has been used to build up a variety of multilayer assemblies on a layer-by-layer basis with precisely controlled thickness and layer sequences.[12−17] By an analogous alternate immersion scheme, multilayered molecular assemblies composed of some POMs and large water-soluble cationic species were built up.[4a,18,19a,b] Commonly, adsorption of first-layer POMs on bare electrodes is a key basis of multilayer growth in the above CMEs. Thus the adsorption strength must be crucial to the stability of the multilayers and even to the possibility of further modifications. The compounds able to adsorb strongly on electrodes are typically some heteropolymolybdates, which are limited, in a relatively small scope, among the large family of POMs. Moreover, the exact adsorption mechanisms have not been fully understood yet.[4a] Therefore, it is of substantial interest to develop a general modification strategy suitable for all POMs. It should have the merits that composition, thickness, and physicochemical properties of the resulting CMEs are well-defined as well as controllable and adjustable to meet practical needs. Recently, Kunitake et al. prepared multilayer films consisting of an octamolybdate anion on some precursor polyelectrolyte films that were essential for forming smooth and uniformly charged surfaces and for the subsequent reproducible adsorption of the anion layers.[20] More recently, Sun et al. reported preliminary electrochemical results of multilayers containing 1:12 phosphomolybdic anions on a precursor aminoethanethiol SAM.[19c] Undoubtedly, alkanethiol SAMs can provide more uniform and better-organized precursor films than the polyelectrolyte films. To our knowledge, however, no detailed studies have been published, until now, on preparation and characterization of multilayers suitable for nearly all POMs on precursor alkanethiol SAMs.

In this article, we describe a novel strategy for the controlled fabrication of well-defined monolayer and multilayer films containing POMs on Au electrodes covered with alkanethiol SAMs. As a representative, monolayer and multilayer self-assemblies consisted of a Keggin-type HPAs $SiMo_{11}VO_{40}^{5-}$ (abbreviated as $SiMo_{11}V$) are elucidated in detail. The composite films are fabricated on the basis of an electrostatic interaction between $SiMo_{11}V$ and a cationic polymer of quaternized poly(4-vinylpyridine) partially complexed with osmium bis(2,2′-bipyridine) chloride (abbreviated as QPVP-Os). In contrast with the commonly used method of immersion growth, a new method of electrochemical growth has been first developed for film formation. The resulting composite films are thoroughly characterized by cyclic voltammetry, UV−vis, XPS, FTIR-RA, and EQCM. Relative to previous strategies,[4a,18,19] our strategy is attractive in that it is a general one suitable for anchoring nearly all kinds of POMs, including those unable to be modified by the previous strategies.

2. Experimental Section

2.1. Chemicals. The $SiMo_{11}VO_{40}^{5-}$ anion was prepared by a published procedure,[21a,b] and its free acid $H_5SiMo_{11}VO_{40}$ was isolated from the reaction mixture by the "etherate" method.[1a] $H_5SiMo_{11}VO_{40}$ was identified in the solid state by IR spectroscopy and in solution by CV and UV−vis spectroscopy. Dawson-type α-$K_6P_2W_{18}O_{62}$ was prepared and characterized in the manner noted in ref 21c; lanthanide complex $K_{10}H_3[Pr(SiMo_7W_4)_2]$ as in ref 21d; and isopolymolybdate $Mo_8O_{26}^{4-}$ as in ref 21e. $H_4SiW_{12}O_{40}$ was purchased from Beijing Xinhua Chemical Co. (China). QPVP-Os was synthesized and characterized according to the published procedures[21f,g] and provided by Professor Xi Zhang (Jilin University, China). Cysteamine (denoted as Cyst) was purchased from Sigma, and 3-mercaptopropionic acid (denoted as MPA) from Aldrich. All of the

(4) (a) Kuhn, A.; Anson, F. C. *Langmuir* **1996**, *12*, 5481. (b) Rong, C.; Anson, F. C. *Anal. Chem.* **1994**, *66*, 3124. (c) Rong, C.; Anson, F. C. *Inorg. Chim. Acta* **1996**, *242*−*243*, 1. (d) Shiu, K.-K.; Anson, F. C. *J. Electroanal. Chem.* **1991**, *309*, 115.

(5) (a) Bidan, G.; Genies, E. M.; Lapkowski, M. *J. Electroanal. Chem.* **1998**, *251*, 297. (b) Bidan, G.; Genies, E. M.; Lapkowski, M. *Synth. Met.* **1989**, *31*, 327. (c) Lapkowski, M.; Bidan, G.; Fournier, M. *Synth. Met.* **1991**, *41*−*43*, 407 and 411. (d) Fabre, B.; Bidan, G.; Lapkowski, M. *J. Chem. Soc., Chem. Commun.* **1994**, 1509. (e) Fabre, B.; Bidan, G. *Electrochim. Acta* **1997**, *42*, 2587.

(6) (a) Pham, M.-C.; Moslih, J.; Chauveau, F.; Lacaze, P.-C. *J. Appl. Electrochem.* **1991**, *21*, 902. (b) Pham, M.-C.; Bouallala, S.; Le, L. A.; Dang, V. M.; Lacaze, P. C. *Electrochim. Acta* **1997**, *42*, 439.

(7) Papadakis, A.; Souliotis, A.; Papaconstantinou, E. *J. Electroanal. Chem.* **1997**, *435*, 17.

(8) Bond, A. M.; Cooper, J. B.; Marken, F.; Way, D. M. *J. Electroanal. Chem.* **1995**, *396*, 407.

(9) Bain, C. D.; Troughton, E. B.; Tao, Y. T.; Evall, J.; Whitesides, G. M.; Nuzzo, R. G. *J. Am. Chem. Soc.* **1981**, *111*, 321 and references therein.

(10) Ulman, A. *Chem. Rev.* **1996**, *96*, 1533.

(11) (a) Lee, H.; Kepley, L. J.; Hong, H.-G.; Mallouk, T. E.; *J. Am. Chem. Soc.* **1988**, *110*, 618. (b) Netzer, L.; Sagiu, J. *J. Am. Chem. Soc.* **1983**, *105*, 674. (c) Tillman, N.; Ulman, A.; Penner, T. L. *Langmuir* **1989**, *5*, 101. (d) Li, D.; Ratner, M. A.; Marks, T. J. *J. Am. Chem. Soc.* **1990**, *112*, 7389. (e) Brust, M.; Blass, P. M.; Bard, A. J. *Langmuir* **1997**, *13*, 5602. (f) Freeman, T. L.; Eavans, S. D.; Ulman, A. *Thin Solid Films* **1994**, *244*, 784.

(12) (a) Decher, G.; Hong, J. D.; Schmitt, J. *Thin Solid Films* **1992**, *210*−*211*, 831. (b) Lvov, Y.; Decher, G.; Mohwald, H. *Langmuir* **1993**, *9*, 481. (c) Vecher, G.; Lvov, Y.; Schmitt, J. *Thin Solid Films* **1994**, *244*, 772.

(13) (a) Ferreira, M.; Cheung, J. H.; Rubner, M. F. *Thin Solid Films* **1994**, *244*, 806 and 985. (b) Ferreira, M.; Rubner, M. F. *Macromolecules* **1995**, *28*, 7170. (c) Fou, A. F.; Rubner, M. F. *Macromolecules* **1995**, *28*, 7115.

(14) Laurent, D.; Schlenoff, J. B. *Langmuir* **1997**, *13*, 1552.

(15) Tien, J.; Terfort, A.; Whitesides, G. M. *Langmuir* **1997**, *13*, 5349.

(16) Araki. K.; Wagner, M. J.; Wrighton, M. S. *Langmuir* **1996**, *12*, 5393.

(17) Zhang, X.; Gao, M.; Kong, X.; Sun, Y.; Shen, J. *J. Chem. Soc., Chem. Commun.* **1994**, 1055.

(18) Ingersoll, D.; Kulesza, P. J.; Faulkner, L. R. *J. Electrochem. Soc.* **1994**, *141*, 140.

(19) (a) Sun, C.; Zhao, J.; Xu, H.; Sun, Y.; Zhang, X.; Shen, J. *J. Electroanal. Chem.* **1997**, *435*, 63. (b) Sun, C.; Zhang, J. *Electroanalysis* **1997**, *9*, 1365. (c) Sun, C.; Zhang, J. *Electrochim. Acta* **1998**, *43*, 943.

(20) Ichinose, I.; Tagawa, H.; Mizuki, S.; Lvov, Y.; Kunitake, T. *Langmuir* **1998**, *14*, 187 and references therein.

(21) (a) Altenau, J. J.; Pope, M. T.; Prados, R. A.; So, H. *Inorg. Chem.* **1975**, *14*, 417. (b) Tourne, C.; Tourne, G. *Bull. Soc. Chim. Fr.* **1969**, 1124. (c) Wu, H. *J. Biol. Chem.* **1920**, *43*, 189. (d) Zhou, B.; Shan, Y.; Liu, Z.; Zhang, X. *J. Inorg. Chem. (Chinese)* **1992**, *8*, 315. (e) Aveston, J.; Anacker, E. W.; Johnson, J. S. *Inorg. Chem.* **1964**, *3*, 735. (f) Aoki, A.; Rajagopalan, R.; Heller, A. *J. Phys. Chem.* **1995**, *99*, 5102 and references therein. (g) Doherty, A. P.; Forster, R, J.; Smyth, M. R.; Vos, J. G. *Anal. Chim. Acta* **1991**, *255*, 45.

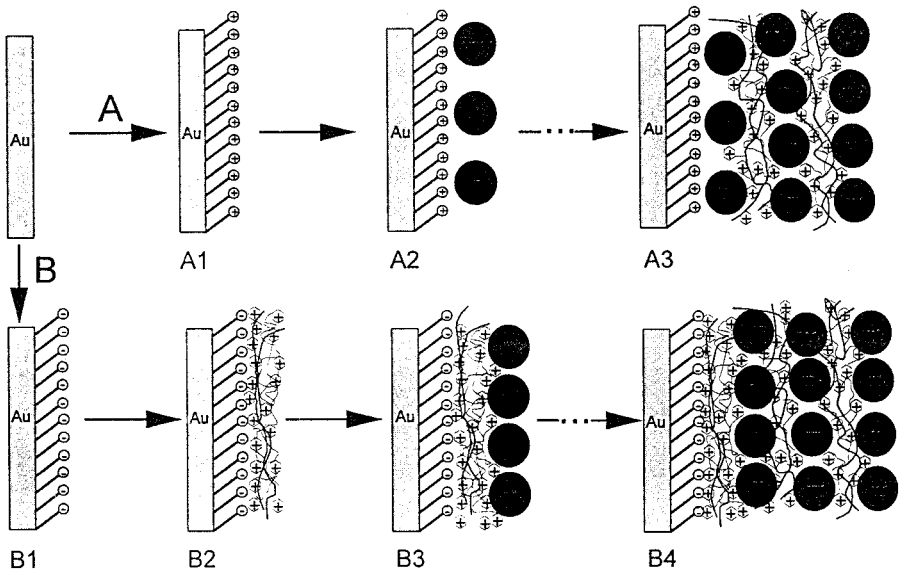

Figure 1. Schematic illustration of deposition procedures and conceptual models of monolayers and multilayers consisted of POMs (large circles) and QPVP-Os (thin curves) on two kinds of positively and negatively charged precursor alkanethiol SAMs. Cysteamine (A) and 3-mercaptopropionic acid (B) SAMs on Au electrodes are typically used. Depicted are various stages of the film formation: (A1) Au/Cyst; (A2) Au/Cyst/POMs; (A3) Au/Cyst/3POMs/2QPVP-Os; (B1) Au/MPA; (B2) Au/MPA/QPVP-Os; (B3) Au/MPA/QPVP-Os/POMs; and (B4) Au/MPA/3QPVP-Os/3POMs.

other chemicals were of reagent grade and used as received. Solutions were prepared from water that had been purified through an Ultrapure water system Milli-Q Plus (Millipore Co.). Its resistivity was over 18 MΩ cm. Buffer solutions were prepared from 0.1 M $NaHSO_4$ (pH 1−3) and 0.1 M NaAc + HAc (pH 4−6). A 0.2 M Na_2SO_4 solution was used as the supporting electrolyte. All solutions were deaerated with pure nitrogen before used.

2.2. Electrochemical Measurements. Electrochemical experiments were performed with a CHI 600 voltammetric analyzer (CH Instruments, USA) in a conventional three-electrode cell. The working electrodes (WE) used in modification of monolayer and multilayer films were homemade polycrystalline gold (Au) disk electrodes, except a glassy carbon electrode (GCE) was used in the investigation of the electrochemical behavior of $SiMo_{11}V$ in solution. The surfaces of WE were polished with 1.0, 0.3, and 0.05 μm α-Al_2O_3 powder successively and washed ultrasonically in water. The gold electrodes were subjected to cyclic potential sweeps between −0.2 and 1.5 V in 1 M H_2SO_4 until a stable CV was obtained. The real areas of Au electrodes were calculated by dividing charge of the reduction peak resulting from Au oxide by 293 μC cm^{-2}.[22] A twisted platinum wire was used as the counter electrode (CE); and a Ag/AgCl (in saturated KCl solution) was used as the reference electrode (RE), against which all potentials were measured and reported in this article. Formal potentials (E_f) of redox couples in CVs were estimated as average values of anodic (E_{pa}) and cathodic (E_{pc}) peak potentials, i.e., $E_f = (E_{pa} + E_{pc})/2$; and peak potential separations $\Delta E_p = E_{pa} - E_{pc}$.

2.3. Procedures of Modification. Figure 1 shows a schematic illustration of deposition procedures and conceptual models of monolayers and multilayers consisting of POMs and QPVP-Os on two kinds of positively and negatively charged precursor alkanethiol SAMs, with cysteamine (A) and 3-mercaptopropionic acid (B) as typical representatives. For modification of the alkanethiol SAMs, clean Au electrodes were immersed in freshly prepared 10 mM Cyst or MPA solutions overnight. The SAMs Au/Cyst and Au/MPA were then ready for further modification by removing them from the solutions and rinsing them with copious amounts of water.

There were two methods used in this article for formation of monolayers and multilayers, i.e., the commonly used immersion growth [4,18,19] and the electrochemical growth developed by us. For modification of $SiMo_{11}V$ monolayer by the electrochemical growth, an Au/Cyst electrode was placed in 2 mM $SiMo_{11}V$ + 0.1 M H_2SO_4 solution; and at the same time cyclic potential sweeps (CPS) were conducted in a potential range between −0.15 and 0.65 V at a scan rate of 100 mV/s for 25 cycles. Au/MPA was first placed in QPVP-Os solution and modified with a QPVP-Os layer by CPS similar to the above; the Au/MPA/QPVP-Os was then placed in $SiMo_{11}V$ solution and modified with a $SiMo_{11}V$ layer. The resulting electrodes (Au/Cyst/$SiMo_{11}V$ and Au/MPA/QPVP-Os/$SiMo_{11}V$) were thoroughly washed with water and ready for characterization. The choice of CPS for 25 cycles was enough for the modification of $SiMo_{11}V$ monolayer since the CPS for more cycles did not increase the peak currents at all. In contrast to immersion growth, independent experiments of immersing the Au/Cyst electrodes in the same $SiMo_{11}V$ solution for different periods showed that their peak currents did not increase until the immersion time was ∼3 h. Obviously the electrochemical growth is more effective than the immersion growth.

For modification of $SiMo_{11}V$ multilayers by the electrochemical growth, its monolayer CMEs were placed alternately in QPVP-Os and $SiMo_{11}V$ solutions; and in each solution the CPS were simultaneously conducted. Between each modification, the resulting electrode was only washed with copious amounts of water, without the drying steps that were commonly required and used in previous methods.[18,19] Thus the $SiMo_{11}V$ multilayer CMEs with different thickness were readily obtained by choice of different cycles of the modification steps.

2.4. UV−Vis Measurements. UV−vis absorbance spectrometric experiments were carried out with a DMS-90 UV−vis spectrophotometer (Varian Inst. Co., Palo Alto, CA). UV−vis spectra of free QPVP-Os and $SiMo_{11}V$ were first measured in 0.1 M H_2SO_4 solution within a quartz cuvette to determine a suitable wavelength scope for featuring the absorption of the two modifiers. For UV−vis measurements of multilayer films, a quartz slide silanized in 5% 3-aminopropyltrimethoxysilane solution for 4 h was used according to a published procedure.[23a] The aminopropylsilanated (abbreviated as APS) quartz slide

(22) Sagara, T.; Kawamura, H.; Nakashima, N. *Langmuir* **1996**, *12*, 4253.

(23) (a) Haller, I. *J. Am. Chem. Soc.* **1978**, *100*, 8050. (b) So, H.; Pope, M. T. *Inorg. Chem.* **1972**, *11*, 1441.

was stored in 0.1 M HCl for use. The multilayer films were fabricated by immersing the APS quartz substrate alternately in $SiMo_{11}V$ and QPVP-Os solutions for ~3 h. After each immersion step, the resulting films were washed with water, dried under nitrogen, and used to record UV−vis spectra to follow the deposition processes. The spectra were background subtracted from a reference sample of a naked quartz slide.

2.5. XPS Measurements. XPS measurements were conducted with an ESCALAB MK II spectrometer (VG Co., U.K.) with a Mg Kα radiation ($h\gamma = 1253.6$ eV) as the X-ray source and a pass energy of 50 eV. The pressure inside the analyzer was maintained at 10^{-9} Torr. The charging calibration was performed by referring the C 1s to the binding energy at 284.6 eV. The resolution of the spectrometer was 0.2 eV. Argon ion sputtering was performed under an accelerating voltage of 2 kV over an area of 1 cm^2. For each sample, a survey scan was recorded followed by high-resolution spectra of individual elements. The monolayer and multilayer films used for XPS measurements were fabricated on polycrystalline gold wafers or gold films which were cleaned in a hot "piranha" solution (H_2SO_4:H_2O_2 = 7:3)[24] for ~15 min, and then thoroughly washed with copious amounts of water. **[Note: Piranha solution is a strong oxidant and must be used with extreme caution.]** Data analysis was based on deconvolution of a high-resolution composite XPS peak into peaks of the individual species in different oxidation states. The deconvolution was carried out by a nonlinear regression analysis provided by the instrument, with position, height, and width of each individual Gaussian peak as variable parameters. The criterion for the best fit was the good agreement between the experimental points and fitted curves.

2.6. FTIR-RA Measurements. FTIR-RA measurements were performed using a Nicolet Avatar 360 spectrometer equipped with a conjugated IR inspector microscopic accessory and a liquid nitrogen cooled mercury−cadmium−telluride (MCT) detector. A spectral range of 4000 to 400 cm^{-1}, 256 scans, and an effective resolution of 1 cm^{-1} were used. The monolayer and multilayer films used here were similarly prepared as those for the XPS measurements. The spectra were background subtracted from a reference sample of a freshly cleaned gold wafer.

2.7. EQCM Measurements. Mass changes were monitored by EQCM (Wuhan University, China) during the electrochemical growth of multilayer films and their subsequent redox processes in supporting electrolyte. Au-coated AT cut quartz crystals (9 MHz) with a geometric area of 0.196 cm^2 were used. The EQCM measurements were conducted in a ~1 mL homemade cell and shielded in a Faraday cage. The system calibration constant (C) of the instrument was 0.178 Hz cm^2 ng^{-1}. Control and data accumulation were carried out by a personal computer.

3. Results and Discussion

3.1. Deposition of Monolayers of $SiMo_{11}V$. The electrochemical behavior of $SiMo_{11}V$ in aqueous solution was investigated and is briefly described here for comparison. In potential range of 0.8 to −0.1 V, CVs of 4.4 mM $SiMo_{11}V$ in 0.5M H_2SO_4 on a GCE show four main redox waves with E_f at 0.518, 0.258, 0.168, and 0.016 V, respectively. And their ΔE_p are 66, 42, 43, and 33 mV close to theoretical values of one-electron (60 mV) and two-electron (30 mV) redox processes.[25a] Therefore, the four redox waves correspond to a one-electron vanadium ($V^{5+/4+}$) and three two-electron molybdate ($Mo^{6+/5+}$) redox reactions of $SiMo_{11}V$.[1a] The fact that peak currents are linearly proportional to the square root of scan rates indicates that the four redox waves are diffusion-controlled redox processes.

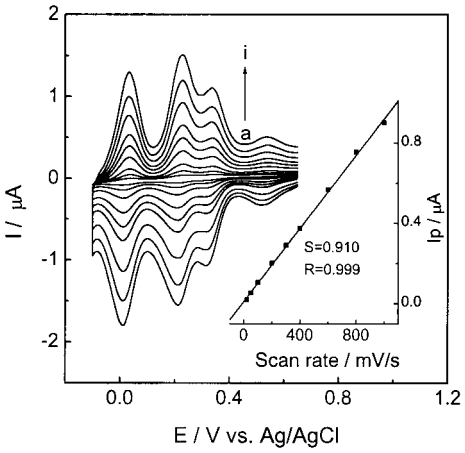

Figure 2. CVs of a monolayer CME of Au/Cyst/$SiMo_{11}V$ in 1.0 M H_2SO_4 at different scan rates of (a) 20, (b) 50, (c) 100, (d) 200, (e) 300, (f) 400, (g) 600, (h) 800, and (i) 1000 mV/s, respectively. The monolayer CME was prepared by the electrochemical growth. The inset shows a relationship of the scan rates vs the fourth reduction peak currents.

Figure 2 shows CVs in 1 M H_2SO_4 at different scan rates of Au/Cyst/$SiMo_{11}V$ fabricated by the electrochemical growth. $SiMo_{11}V$ in the CME exhibits four couples of symmetrical redox waves with E_f at 0.53, 0.33, 0.22 and 0.023 V, which are similar to those of $SiMo_{11}V$ in solution considering pH effect and also assigned to one one-electron vanadium ($V^{5+/4+}$) and three two-electron molybdenum ($Mo^{6+/5+}$) redox processes, respectively. The peak currents are proportional to scan rates up to 1000 mV/s, as shown in the inset of Figure 2, taking the fourth reduction peak as a representative. Moreover, the E_fs are largely independent of scan rates and the ΔE_p are as small as ca. 20−25 mV, suggesting that the electron-transfer processes are fairly fast. The peak potential full width at half-maximum of peak current, E_{fwhm}, is ~77 mV for the fourth well-resolved reduction peak at a scan rate of 200 mV/s, which is slightly larger than the theoretically predicted value (90/n) of 45 mV for ideal two-electron surface waves.[25b] This may result from some interactions between $SiMo_{11}V$ anions in the film. In brief, the Au/Cyst/$SiMo_{11}V$ CME undergoes four couples of reversible surface processes, which is consistent with the electrochemical behavior of surface-confined HPAs.[2−6]

Calculated from linear sweep voltammetry at low scan rates, the apparent surface coverages of $SiMo_{11}V$ immobilized on Au/Cyst electrodes are $6-9 \times 10^{-11}$ mol/cm^2 on the basis of the practical areas of the gold electrodes. The maximum surface coverage could be 1.4×10^{-10} mol/cm^2, if $SiMo_{11}V$ is closely packed to full coverage, by taking an approximate diameter of the spherical HPA as 1.2 nm.[18,27] Thus the apparent surface coverages of the Au/Cyst/$SiMo_{11}V$ CMEs are only a fractional full coverage (43−64%). However, considering the possibly high Coulombic repulsion among the nega-

(24) Pintchovski, F.; Price, J. B.; Tobin, P. J.; Peavey, J.; Kobold, D. *J. Electrochem. Soc.* **1987**, *109*, 3559.

(25) (a) Bard, A. J.; Faulkner, L. R. *Electrochemical Methods. Fundamentals and Applications*; John Wiley & Sons: New York, 1980. (b) Murray, R. W. In *Electroanalytical Chemistry*; Bard, A. J., Ed.; Marcel Dekker: New York, 1984; Vol. 13, pp 191−368.

(26) Xi, X.; Wang, B.; Liu, B.; Dong, S. *Electrochim. Acta* **1995**, *40*, 1025.

(27) Rocchiccioli-Deltcheff, C.; Fourmier, M.; Franck, R.; Thouvenot, R. *Inorg. Chem.* **1983**, *22*, 207.

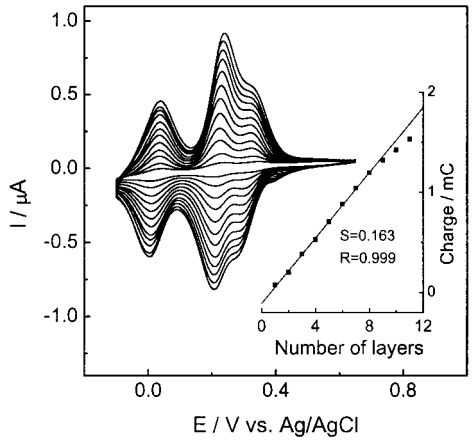

Figure 3. CVs of multilayer CMEs of Au/Cyst/nSiMo$_{11}$V/($n-1$)QPVP-Os in 1.0 M H_2SO_4 with increase in number of layers from $n = 1$ to 12 (shown from inside to outside curves), respectively. Scan rate: 20 mV/s. These CMEs were prepared by the electrochemical growth. The inset shows a relationship of the number of layers vs the integrated charges under the third two-electron reduction peaks.

tively charged SiMo$_{11}$V, we think that the Au/Cyst/SiMo$_{11}$V CMEs are at the level of submonolayer-to-monolayer coverages.

3.2. Layer-by-Layer Growth of Multilayers Consisting of SiMo$_{11}$V and QPVP-Os. Figure 3 shows a set of CVs in 1 M H_2SO_4 exhibited by Au/Cyst/nSiMo$_{11}$V/($n-1$)QPVP-Os multilayers with SiMo$_{11}$V as outmost layers at different layer numbers from $n = 1$ to 12. A good linear relationship between the layer numbers and the charges under the third two-electron reduction peaks of SiMo$_{11}$V, as shown in the insert of Figure 3, demonstrates that the electrochemical growth gives uniform and homogeneous multilayers. In addition, the deviation from the line when the layer number greater than 10 may not necessarily suggest the multilayer growth become nonuniform because the electroactivity of SiMo$_{11}$V loaded in the outside layers must be largely affected by the distance between the electroactive sites and the electrode surface. In contrast, the immersion growth induces relatively extensive deposition during the first two immersion cycles.[18] The slope of 0.1634 mC per SiMo$_{11}$V layer gives an averaged increase in surface coverage of $\sim 1.15 \times 10^{-10}$ mol/cm^2, which roughly corresponds to addition of a SiMo$_{11}$V monolayer after each growth. It is noteworthy that the surface coverage of a SiMo$_{11}$V layer on a QPVP-Os layer is slightly larger than that on a cysteamine SAM, which must relate to the fact that the polymeric QPVP-Os provides not only more cationic binding sites but also a wider practical area for deposition of SiMo$_{11}$V than the cysteamine SAM.

By using the electrochemical growth, stable and reproducible multilayer structures have been obtained readily and rapidly without drying steps. The aim of the use of 0.1 M H_2SO_4 in both SiMo$_{11}$V and QPVP-Os solutions is to maintain a stable pH condition for SiMo$_{11}$V as well as to serve as supporting electrolyte during CPS in the electrochemical growth. The extent of possible competition adsorption from electrolyte ions during the electrochemical growth is exactly negligible as evidenced by XPS studies (see part 3.4).

3.3. Comparison of the Electrochemical Growth and the Immersion Growth. Figure 4 shows CVs in 1 M H_2SO_4 of Au/Cyst/SiMo$_{11}$V (solid line), Au/Cyst/SiMo$_{11}$V/QPVP-Os (dash line) in plots A and B and Au/Cyst/5SiMo$_{11}$V/4QPVP-Os (solid line), Au/Cyst/5SiMo$_{11}$V/5QPVP-Os (dash line) in plots C and D prepared by the electrochemical growth (A, C) and the immersion growth (B, D). By comparing these CVs, several remarks can be made as follows:

(1) Some remarkable difference exist in the electrochemical behavior of monolayers and multilayers fabricated by the two different methods. After the electrochemical growth of a QPVP-Os layer on top of a SiMo$_{11}$V layer, the shape and width as well as height and symmetry of the redox peaks exhibited by the inner SiMo$_{11}$V remain little affected (Figure 4A and C), which suggests that the outermost QPVP-Os layer might be thin and uniform enough to show no significant effect on the counterion transfer necessary for redox processes of SiMo$_{11}$V. However, a QPVP-Os layer deposited by the immersion growth evidently makes the redox peak shape ill-defined, the symmetry becomes poor (ΔE_p increased), and the peak current decreased (Figure 4B and D), which suggests a greater effect probably due to formation of a relatively thick, nonhomogeneous QPVP-Os layer.

(2) The less significant response from $V^{5+/4+}$ of SiMo$_{11}$V when modified in multilayers, like those in Figure 3 and Figure 4C and D, is due to some effects of QPVP-Os layers, which can be evidenced by the fact of a decrease in peak currents of the $V^{5+/4+}$ after deposition of QPVP-Os layers on SiMo$_{11}$V layers (Figure 4A and B). The effects exist similarly in multilayers prepared by the two methods.

(3) The absence of Os(bpy)$_2^{3+/2+}$ response in the multilayers consisted of SiMo$_{11}$V and QPVP-Os, which is expected at $\sim$0.3 V,[21] is probably due to (a) partial overlapping with the first two two-electron redox waves centered on SiMo$_{11}$V, (b) impediment from highly anionic SiMo$_{11}$V layers on the transport of electrons and/or counterions delivered to Os(bpy)$_2^{3+/2+}$,[4a] and (c) a lower concentration of Os(bpy)$_2$ complexed within QPVP-Os. We think that the first factor (a) is the main reason for it because the two couples of well-resolved redox waves among 0.1−0.5 V in monolayers (Figure 4A and B) indeed become overlapped in multilayers (Figure 4C and D). In addition, the response of Os(bpy)$_2^{3+/2+}$ exactly appeared in other POMs-containing multilayers where no redox waves from POMs occur at potentials near 0.3 V (see Figure 10).

3.4. UV−Vis Characterization. UV−vis spectrometry is a useful technique to characterize the growth process of multilayers.[13b,16,17,19b−c] For comparison, it is helpful to refer to the UV−vis spectra of SiMo$_{11}$V and QPVP-Os in solution. As shown in Figure 5A, the UV−vis spectrum of the QPVP-Os solution is noted by two peaks with the maximum absorption wavelength values of 252 and 290 nm and a shoulder at $\sim$224 nm, while that of SiMo$_{11}$V solution shows strong absorption near 200 nm with a weak shoulder at $\sim$242 nm which could be assigned to oxygen−metal charge-transfer bands.[1a,23b] The addition spectrum between the two was also given to show a possible UV−vis spectrum shape of the multilayer films.

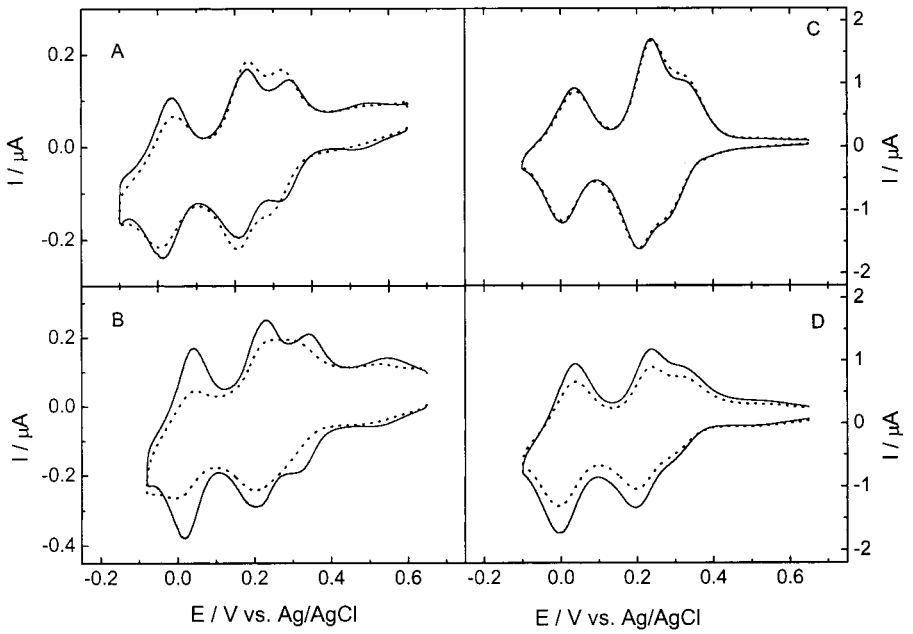

Figure 4. CVs in 1 M H_2SO_4 of Au/Cyst/$SiMo_{11}V$ (solid line), Au/Cyst/$SiMo_{11}V$/QPVP-Os (dash line) in plots A and B and Au/Cyst/5$SiMo_{11}V$/4QPVP-Os (solid line), Au/Cyst/5$SiMo_{11}V$/5QPVP-Os (dash line) in plots C and D prepared by the electrochemical growth (A and C) and the immersion growth (B and D).

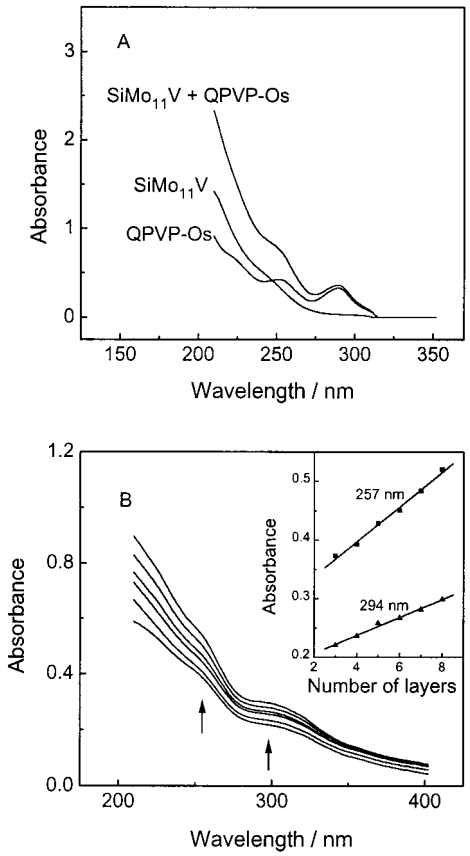

Figure 5. (A) UV−vis spectra of 0.1 M H_2SO_4 solutions containing each of the two modifiers $SiMo_{11}V$ and QPVP-Os as well as an addition spectrum between the two, as noted in the plot. (B) UV−vis spectra of multilayer films fabricated on a silanized quartz slide with increase in number of outmost $SiMo_{11}V$ layers from 3 to 8 (shown from lower to upper curves), respectively. The insert shows relationships of the absorbance at 257 and 294 nm vs the number of multilayers.

Figure 5B shows UV−vis spectra of multilayer films with $SiMo_{11}V$ as outermost layers under different HPA layer numbers. The UV−vis spectra of the multilayer films show three absorption shoulders. Second, differentiating of the spectra shows the three shoulders are peaked at approximately 226, 257, and 294 nm. The linearity of the absorption values at 257 and 294 nm vs the number of layers, as shown in the inset of Figure 5B, suggest a nearly uniform growth of the multilayer films. Since the UV−vis spectra do not show any absorption due to intervalence charge-transfer transition in visible region, all molybdenum atoms of $SiMo_{11}V$ in the multilayer films are at oxidation state of +6 and vanadium at +5, which is in agreement with the XPS results.

3.5. XPS Characterization. XPS measurements were performed to identify composition and characteristics of the monolayer and multilayer films prepared by the immersion growth and the electrochemical growth. High-resolution XPS spectra of C 1s, O 1s, S 2p, Mo 3d, and Os 4f were recorded, and a survey scan in a binding energy (BE) window of 0−1250 eV was taken. The results and analysis of XPS spectra for O 1s and S 2p levels are described as follows, whereas those for the other elements are given in the Supporting Information.

Features of the O 1s and S 2p XPS Spectra. The multilayers prepared by the two methods give two distinctive XPS spectra for the O ls level. Deconvolution of the high-resolution O 1s XPS peaks helps identify various oxygen-containing species present in the multilayers. Three O 1s signals are noticed at BE = 530.3, 531.5, and 532.6 eV in the multilayer films by the immersion growth (Figure 6A), whereas only two O 1s signals appear at BE = 530.5 and 532.3 eV for the multilayer films created by the electrochemical growth (Figure 6B). The lower BE signal (530.4 ± 0.1 eV) is assigned to the oxygen in $SiMo_{11}V$, similar to metal oxide MoO_3 (530.4 eV) and $PMo_{12}O_{40}^{3-}$ (530.5 eV),[28b] and metallic anion H_2MoO_4 (530.5 eV).[28c] The middle BE signal (531.5 eV) is due to SO_4^{2-}.[28a,c] It is remarkable

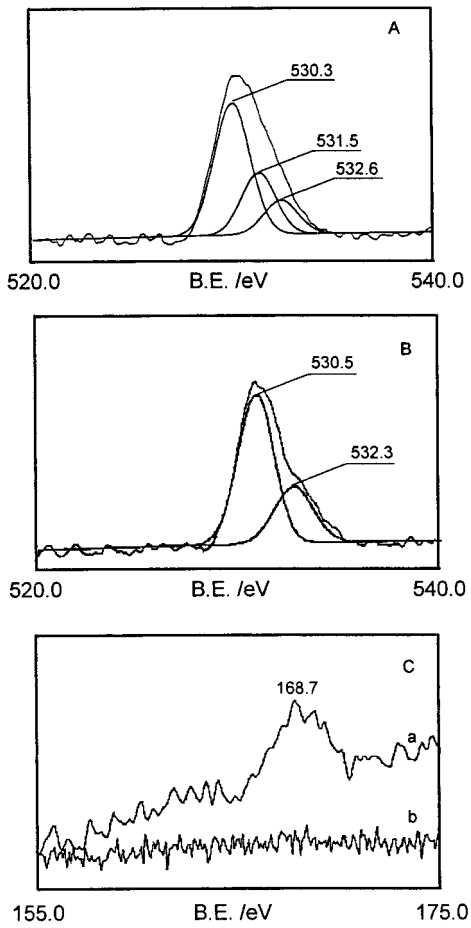

Figure 6. XPS spectra of (A) O 1S energy level for a multilayer film of Au/Cyst/3SiMo$_{11}$V/3QPVP-Os prepared by the immersion growth, (B) O 1S energy level for a multilayer film of Au/Cyst/8SiMo$_{11}$V/7QPVP-Os prepared by the electrochemical growth, and (C) S 2p energy level for the same multilayer films (a) and (b) as those used in Figure 6, parts A and B, respectively.

that SO_4^{2-} is present in the multilayer films prepared by the immersion growth, but not in the multilayer films by the electrochemical growth. The higher BE signal (532.3 ± 0.3 eV) corresponds to chemisorbed water or other stoichiometric hydroxide groups attached to metal centers,[28b–d] which is also proven by the fact that an independent XPS signal at 532.0 eV is always present at Au/Cyst in our experiments. In Figure 6A and B, the signals at the lower BE of ~530.4 eV always have a greater intensity than others. It is consistent with the fact that the SiMo$_{11}$V responsible for the signals is the main component of the multilayers.

The Au/Cyst film exhibits a S 2p XPS signal at 162.5 ± 0.3 eV that is characteristic of thiolates on Au.[31] This S 2p signal is also detectable for thinner multilayer films, but weaker gradually with increasing the number of layers. As for multilayers prepared by the immersion growth, another XPS signal for S 2p level appears at 168.7 ± 0.3 eV, which must be due to SO_4^{2-} (169.1 eV).[28a,d] And relative intensity of the SO_4^{2-} signal becomes larger with the increase in the number of layers to some extent. (A figure is given in the Supporting Information.) However, multilayers prepared by the electrochemical growth do not show any S 2p XPS signals originating from SO_4^{2-}. Figure 6C clearly depicts the difference in XPS spectra for the S 2p level between multilayers of Au/Cyst/3SiMo$_{11}$V/3QPVP-Os prepared by the immersion growth (curve a) and Au/Cyst/8SiMo$_{11}$V/7QPVP-Os by the electrochemical growth (curve b). The difference reproducibly exists regardless of the number of layers. As for multilayers prepared by the electrochemical growth, moreover, no SO_4^{2-} signal was observed in XPS measurements in conjunction with argon (Ar) ion sputtering for different periods.

In brief, both O ls and S 2p XPS spectra prove such a difference between the two different methods for multilayer formation that the immersion growth involves a competition adsorption of SO_4^{2-} from electrolyte solution as reported by Anson et al.,[4a] but the electrochemical growth gives a good selectivity in deposition of SiMo$_{11}$V other than SO_4^{2-}. Possible reasons for the remarkable difference may include the following factors:

(1) The immersion growth involves simple ion-exchange processes driven only by naturally electrostatic attraction between the cationic (QPVP-Os) and anionic (SiMo$_{11}$VO$_{40}^{5-}$ and SO_4^{2-}) species without any other driving forces. So the immersion growth seems not to have significantly selective effects on ions' deposition during film formation.

(2) However, the electrochemical growth may provide at least two additional functions in favor of the multilayer growth. First, a positive electric field is formed in electrode interface by CPS in a positive potential window. It must accelerate and suit the deposition of highly negatively charged SiMo$_{11}$VO$_{40}^{5-}$ than that of SO_4^{2-}. On the other hand, by electrostatic repulsion, it avoids the drawback of overdeposition and formation of thick cationic QPVP-Os layers that is inevitably present in the immersion growth and results in some negative effects on electrochemistry of inner SiMo$_{11}$V layers (as described in part 3.3). Second, redox reactions of HPA ⇔ HPB during CPS should be more adaptable to loading SiMo$_{11}$V other than SO_4^{2-}, since the resulting HPBs are known as complex colloidal species, bearing much higher negative charges.

Depth Profiles of the Multilayer Films. To determine its structural characteristics, a multilayer film of Au/Cyst/9SiMo$_{11}$V/8QPVP-Os prepared by the electrochemical growth is subjected to XPS analysis in conjunction with argon (Ar) ion sputtering for different times. Depth profiles (Figure 7) are obtained in terms of C 1s, Mo 3d, Os 4f, and N 1s levels by taking advantage of

(28) (a) Wagner, C. D.; Riggs, W. M.; Davis, L. E.; Moulder, J. F. In *Handbook of X-ray Photoelectron Spectroscopy*; Chastain, J., Ed.; Physical Electronics Division, Perkin-Elmer: Eden Prairie, MN, 1979. (b) Hasik, M.; Pron, A.; Pozniczek, J.; Bielanski, A.; Piwowarska, Z.; Kruczala, K.; Dziembaj, R. *J. Chem. Soc., Faraday Trans.* **1994**, *90*, 2099. (c) Wagner, C. D.; Zatko, D. A.; Raymond, R. H. *Anal. Chem.* **1980**, *52*, 1445. (d) Ilangovan, G.; Pillai, K. C. *Langmuir* **1997**, *13*, 566.

(29) (a) Weakley, T. I. R. *Sruct. Bond.* **1974**, 18, 131. (b) Wang, E.; Zhang, L.; Shen, E.; Wang, Z.; Lin, Y.; Jin, S. *Sci. China Ser. B* **1992**, *7*, 673.

(30) (a) Pan, W.; Durning, C. J.; Turro, N. J. *Langmuir* **1996**, *12*, 4469. (b) Keita, B.; Nadjo, L.; Belanger, D.; Wilde, C. P.; Hilaire, M. *J. Electroanal. Chem.* **1995**, *384*, 155. (c) Ohtsuka, T.; Wakabayashi, T.; Einaga, H. *J. Electroanal. Chem.* **1994**, *377*, 107. (d) Keita, B.; Mahmoud, A.; Nadjo, L. *J. Electroanal. Chem.* **1995**, *386*, 245. (e) Shimazu, K.; Yagi, I.; Sato, Y.; Uosaki, K. *Langmuir* **1992**, *8*, 1385. (f) Naoi, K.; Lien, M.; Smyrl, W. H. *J. Electrochem. Soc.* **1991**, *138*, 440. (g) Frelink, T.; Visscher, W.; van Veen, J. A. R. *Langmuir* **1996**, *12*, 3702.

(31) Schoenfisch, M. H.; Pemberton, J. E. *J. Am. Chem. Soc.* **1998**, *120*, 4502.

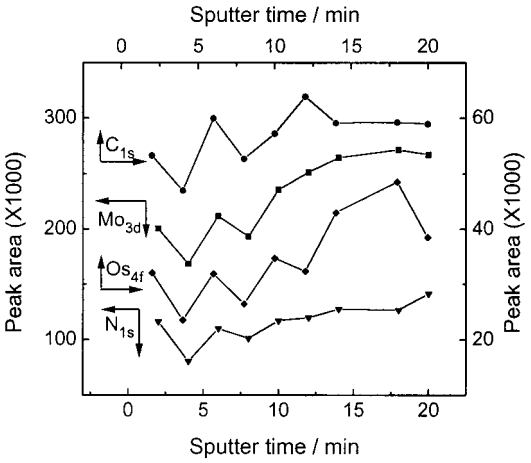

Figure 7. The depth profiles of four elements C, Mo, Os, and N for a multilayer film of Au/Cyst/9$SiMo_{11}V$/8QPVP-Os prepared by the electrochemical growth. The data were obtained by XPS measurements in conjunction with Ar ion sputtering for different times.

integration areas of their XPS peaks as rough estimations for their amounts present in the multilayer. Undoubtedly, the XPS signals of Mo 3d comes from the $SiMo_{11}V$ layers, while those of C 1s, N 1s, and Os 4f are mainly from the QPVP-Os layers. The nearly identical trends of changes in the peak areas, especially in the first several sputtering times, indicate a uniform distribution of $SiMo_{11}V$ and QPVP-Os in the multilayer. Within experimental errors leading to signal oscillations, the same results are also obtained in two other independent XPS measurements. Additionally, it is worth noting that the similar trends of changes in amounts of Mo, C, N, and Os imply that the rigid anion $SiMo_{11}V$ is probably partially entrapped in interior rooms of lithe segments of the polymeric QPVP-Os. Therefore, the boundary between a $SiMo_{11}V$ layer and a QPVP-Os layer could be slightly less distinctive when compared with that of the multilayers consisting of both rigid HPAs and $Os(bpy)_3^{2+}$ or $Ru(bpy)_3^{2+}$ cations.[4a,18] As for multilayer films prepared by the immersion growth, however, only poor results of the depth profiles are obtained. Therefore, the electrochemical growth can fabricate monolayer and multilayer films in a more even and homogeneous way than the immersion growth.

3.6. FTIR-RA Characterization. FTIR spectra of $SiMo_{11}V$ powder show four asymmetrical stretching vibrations of Mo−Od at 960.1 cm^{-1}, Si−Oa at 906.5 cm^{-1}, Mo−Ob−Mo at ∼860 cm^{-1}, and Mo−Oc−Mo at 781.3 cm^{-1}, which are typical features of HPAs with a Keggin structure.[27,29a,b]

FTIR-RA measurements were performed on multilayers at various stages of film formation. We focus mainly in the low-frequency region of 1000−700 cm^{-1} where the featured vibrations of immobilized $SiMo_{11}V$ would appear. FTIR-RA spectra of (a) Au/Cyst, (b) Au/Cyst/$SiMo_{11}V$, (c) Au/Cyst/3$SiMo_{11}V$/2QPVP-Os and (d) Au/Cyst/7$SiMo_{11}V$/6QPVP-Os were recored. (A figure is given in the Supporting Information.) A relatively weak absorbance probably due to very small amounts of $SiMo_{11}V$ present in the ultrathin films is observed. When compared with that of the $SiMo_{11}V$-free SAM of Au/Cyst, however, FTIR-RA spectra of the $SiMo_{11}V$-containing monolayer and multilayer CMEs exhibit

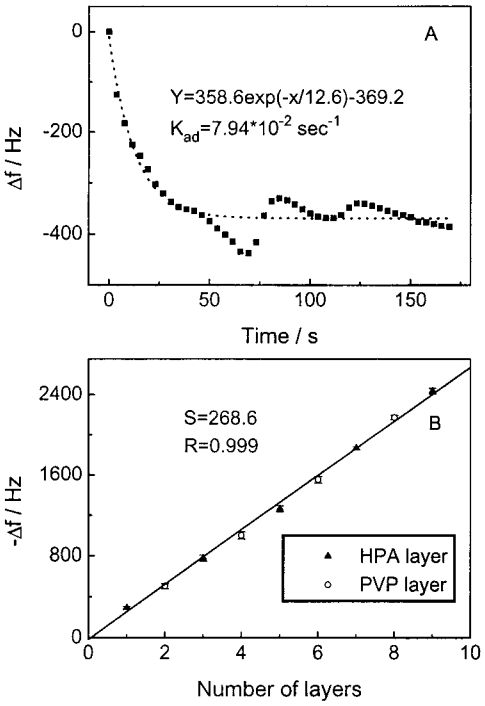

Figure 8. (A) The frequency change depicted the electrochemical growth of a $SiMo_{11}V$ layer onto a Au/Cyst/$SiMo_{11}V$/QPVP-Os CME (see text for detail); and (B) the relationship of the number of layers vs frequency decrements during the alternate electrochemical growth of $SiMo_{11}V$ and QPVP-Os multilayers. Note: The layer numbers shown here were recorded by accumulating those of the $SiMo_{11}V$ and QPVP-Os multilayers together.

some vibration peaks characteristic of $SiMo_{11}V$ at approximately 950, 904−912, 853, and 787−797 cm^{-1}, respectively, although there are some shifts on peak positions. It is noteworthy that the vibration peaks of curves b and c are much closer to those of $SiMo_{11}V$ powder than curve d. Thus, it seems to imply that the $SiMo_{11}V$-containing monolayer as well as thinner multilayers could be less affected than thicker multilayers by the electrostatic interaction upon which the multilayer films are formed. In addition, these widened and shifted peaks could also derive from the strong electrostatic interaction.

3.7. EQCM Characterization. The EQCM is an excellent tool for tracing film formation and ion motion during redox processes.[4a,20,30] In our experiments, the in situ monitoring of mass changes by EQCM was performed during the electrochemical growth of multilayer films and their subsequent redox processes in supporting electrolyte.

Adsorption Kinetic and Multilayer Formation. The electrochemical growth of a $SiMo_{11}V$ layer onto the Au/Cyst/$SiMo_{11}V$/QPVP-Os was examined in situ by EQCM after a careful injection of 1 mL of 0.1 M H_2SO_4 containing 1 mM $SiMo_{11}V$. During the simultaneously conducted CPS from 0.65 to −0.1 V, a steeply decreasing frequency is observed at first and followed by a gradual decrease with a frequency oscillation. Data of frequency changes are culled from each of the CPS at 0.65 V and plotted against proceeding times, as shown in Figure 8A. The resonant frequency stabilizes after ∼50 s. The light frequency oscillation after the first steep decrease may be derived from a dynamic balance between

overloading adsorption and desorption of $SiMo_{11}V$, which was also observed for alkanethiol adsorption on gold.[30a] The frequency shifts during the film growth are fit with an exponential decay and give a simulation curve of $\Delta f = 358.6 \exp(-x/12.6) - 369.2$, from which the adsorption kinetic constant is obtained as 7.94×10^{-2} s^{-1}, assuming a first-order reaction.

Figure 8B shows a relationship of frequency decrements ($-\Delta f$) of QCM resonator during the alternate electrochemical growth of $SiMo_{11}V$ and QPVP-Os multilayers vs number of the layers. The data of $-\Delta f$ are obtained by difference of the frequencies before and after injection of 50 μL of $SiMo_{11}V$ or QPVP-Os solution. The approximately linear relationship between $-\Delta f$ and the number of layers indicates a regular and reproducible growth of $SiMo_{11}V$ and QPVP-Os multilayers, which is in agreement with the results of cyclic voltammetry (Figure 3) and UV−vis spectra (Figure 5). The frequency change of approximately −268.6 Hz corresponds to a mass increase of ∼295.8 ng, which is at the level of monolayer coverage considering high real area of the anchoring layer of polymeric QPVP-Os.

Ion Motions during the Redox Processes of $SiMo_{11}V$. The ion and/or solvent transport during redox processes of POMs is particularly important for better understanding their electrochemical behavior and electrocatalytic properties. However, the EQCM studies on it are fairly few.[30c,d] A typical EQCM measurements was conducted in 0.1 M H_2SO_4 on an Au/Cyst/4$SiMo_{11}V$/3QPVP-Os multilayer prepared by the electrochemical growth. A scan rate is chosen as slow as 10 mV/s to ensure that the redox reactions were under thermodynamic control and free from kinetic or transport effect.[30f] Figure 9A is a frequency response (dash line) recorded simultaneously with corresponding CV (solid line). A frequency increase (mass decrease) occurs during the reduction processes of $SiMo_{11}V$, and a frequency decrease (mass increase) occurs during the reoxidation of the reduced $SiMo_{11}V$. The frequency and current responses are almost reversible, reproducible, and independent of cycles of the CPS. Furthermore, a derivative curve (Figure 9B) of the frequency response shows three couples of peaks excellently tracking the three redox waves of $SiMo_{11}V$. Therefore, we think the frequency response must essentially be derived from ion motions accompanying the redox processes of $SiMo_{11}V$.

From the plot of frequency changes (ΔF) vs charges (Q), an equivalent molar mass (M_{eq}) of the species exchanged during the HPA's redox processes is calculated according to the equation:

$$M_{eq} = (-\Delta FA/C)/(Q/F) \quad (1)$$

where the parameters have their common meanings. In terms of the reduction processes of $SiMo_{11}V$, two straight ΔF vs Q lines 1 and 2 (Figure 9C) are obtained which are tracking exactly the first two and the third reduction processes originated from molybdate−oxo framework of $SiMo_{11}V$, respectively. It is remarkable that the two lines 1 and 2 have different slopes of 0.255 and 0.470 Hz/μC, from which two M_{eq} of −26.8 and −49.6 g/mol are determined by eq 1, respectively.

If only proton permeation into the film is involved in keeping its charge neutrality, a small frequency decrease will be expected. However it does not hold

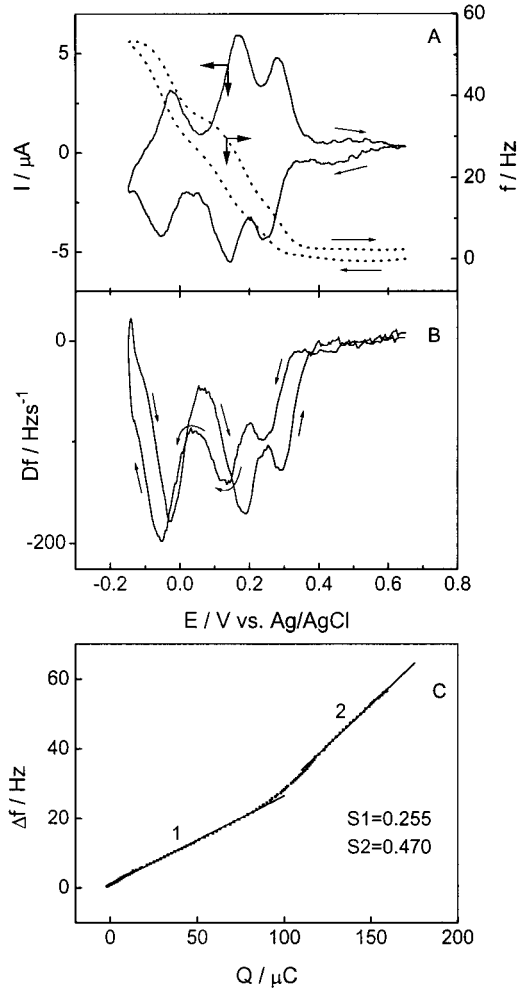

Figure 9. (A) Simultaneously recorded curves of a frequency response (dash line) and a corresponding CV (solid line) of a multilayer CME Au/Cyst/4$SiMo_{11}V$/3QPVP-Os in 0.1 M H_2SO_4. Scan rate: 10 mV/s. The multilayer CME was prepared by the electrochemical growth. (B) The derivative curve of the frequency response. (C) The relationships of the frequency changes (ΔF) vs the reduction charges (Q) (data obtained from Figure 9A).

because of the large frequency increases present here. On the other hand, M_{eq} will be −97 g/mol only if the release of the electrolyte anion HSO_4^-, which is believed to be the main anion present in 0.1 M H_2SO_4 in view of its molarity, is involved.[30g] But it is much smaller than our experimental values. Therefore mixed ion motions are probably more reasonable in maintenance of the charge neutrality of a complex system, which is not unexpected.[30c−g] We assume that a proton is accompanied by one molecule of water, i.e., forming a hydronium ion H_3O^+, which should not be far from the exact situation.[30c] Thus HSO_4^- and H_3O^+ are supposed to be the two main anion and cation provided by 0.1 M H_2SO_4, respectively. If we take x for the transport number of HSO_4^- and $(1 - x)$ for H_3O^+, then the mass balance should be depicted by

$$M_{eq} = 19(1 - x) - 97x \quad (2)$$

From eq 2, the transport numbers of permeating ions into or out of the multilayer during the reduction processes of $SiMo_{11}V$ can be estimated. As for the first two reduction processes where $M_{eq} = -26.8$ g/mol, the

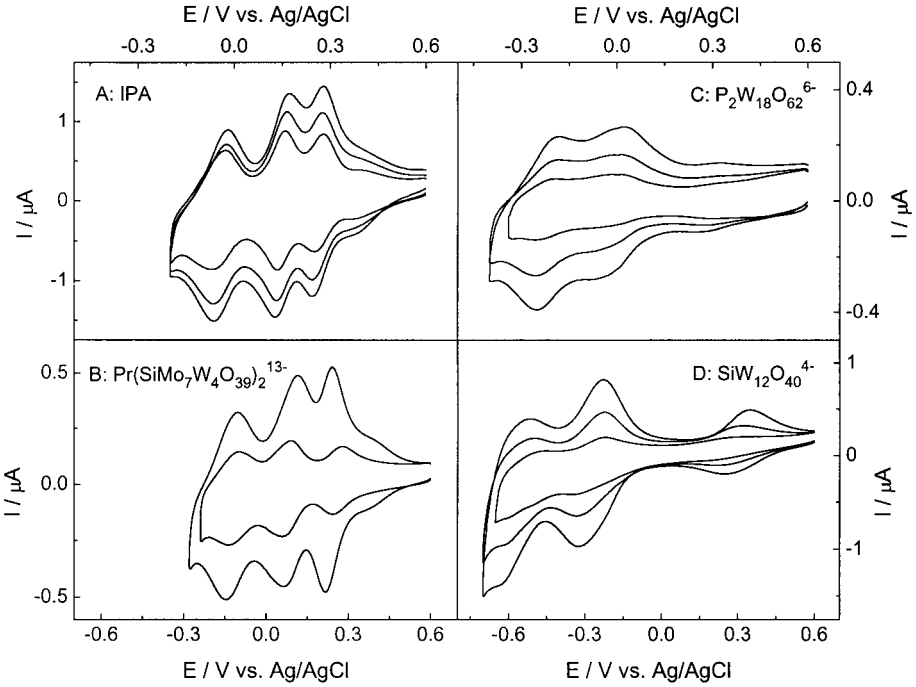

Figure 10. CVs of (A) Au/Cyst/$n$$Mo_8O_{26}^{4-}$/($n$−1)QPVP-Os ($n$ = 2, 3, 4) in 0.1 M H_2SO_4, (B) Au/Cyst/$n$$Pr(SiMo_7W_4O_{39})_2^{13-}$/($n$−1)-QPVP-Os ($n$ = 1, 2) in pH 1.53 buffer solution, (C) Au/MPA/nQPVP-Os/$n$$P_2W_{18}O_{62}^{6-}$ (n = 1, 2, 3) in pH 3.06 buffer solution and (D) Au/Cyst/$n$$SiW_{12}O_{40}^{4-}$/($n$−1)QPVP-Os ($n$ = 2, 4, 6) in pH 4.6 buffer solution. These composite films were prepared by the electrochemical growth. Scan rate: 0.1 V/s.

charge neutrality is maintained by 40% release of HSO_4^- and 60% uptake of H_3O^+; while as for the third one where M_{eq} = −49.6 g/mol, 59% release of HSO_4^- and 41% uptake of H_3O^+ is involved. In contrast to previous EQCM results that a proton was reported to be the main permeating species through polymer films doped with HPAs,[30c,d] we give here the first EQCM evidence that the electrolyte anion also plays an equally important role with proton. To our knowledge, different transport numbers of the same kind of permeating species in the mixed ion motions at different stages of the HPA's reduction processes are reported for the first time. Detailed EQCM studies on the mixed ion motions were also performed. Different ratios of the transport numbers of HSO_4^- and H_3O^+ were obtained from the continuous presence of two distinct segments of $\Delta F-Q$ lines, similar to those in Figure 9C. The relative contribution of the two permeating ions depends on scan rate, film structure, and supporting electrolyte, which will be elaborated in detail later.

3.8. Stability Tests. The monolayer and multilayer CMEs prepared by the electrochemical growth were subjected to rigorous stability tests. Organothiol SAMs on Au exposed to air for a prolonged period were reported to be oxidized to sulfites or sulfates which would desorb and result in a poor stability.[31] However, negligible changes of the electrochemical behavior are found when the CMEs are exposed in air or soaked in supporting electrolyte for several months. The CMEs quickly obtain a steady-state CV and keep it identical for thousands of cycles during CPS over a potential window where only the first four redox waves of $SiMo_{11}V$ appear. When CPS extend to a more positive potential where oxidation of both Au and alkanethiols will significantly occur, the monolayer CMEs do become ill-defined in CV shapes and decrease in peak currents, but the multilayer CMEs retain their CVs unchanged. In addition, pH effects on stability of the CMEs were also checked. Under extreme conditions, e.g., in pH 7 phosphate buffer, peak shapes become ill-defined and peak currents decrease gradually with CPS proceeding. Possible reasons may include (a) weakened electrostatic interaction between cationic and anionic layers and (b) decomposition of $SiMo_{11}V$ by OH^- ions in the neutral solution. However the former reason seems to be unlikely or less important at least here since the cysteamine SAMs must keep their positively charged states due to their pK_b = 1.7.[32] Thus the later reason is mainly responsible for the poor stability in neutral solution. However, under acidic conditions where $SiMo_{11}V$ is stable, peak currents of the CMEs are little affected.

In conclusion, the multilayer CMEs prepared by the electrochemical growth have an excellent stability. It must derive from the sound and homogeneous multi-layered structure between the rigid inorganic layers of $SiMo_{11}V$ and the lithe polymeric layers of QPVP-Os that resembles cross-linked polymers of high physicochemical stability.[18]

3.9. Generality of the Modification Strategy. Figure 10 shows some selected CVs of composite films containing (A) $Mo_8O_{26}^{4-}$ in 0.1 M H_2SO_4, (B) $Pr(SiMo_7W_4O_{39})_2^{13-}$ in pH 1.53 buffer solution, (C) $P_2W_{18}O_{62}^{6-}$ in pH 3.06 buffer solution, and (D) $SiW_{12}O_{40}^{4-}$ in pH 4.6 buffer solution. Similar to the composite films containing $SiMo_{11}V$ as described above, the composite films shown in Figure 10 also exhibit excellent stability and well-defined reversible electrochemical behavior of the POMs themselves, respectively. In addition, it is noteworthy that a distinctive response appeared at ∼0.3 V in $SiW_{12}O_{40}^{4-}$ -containing multilayers (Figure 10D). It must be derived from the redox reaction of

(32) Zhao, J.; Yu, H.; Wang, Y.; Liu, Z. *Chem. J. Chinese Univ.* **1998**, *19*, 464.

$Os(bpy)_2^{3+/2+}$ complexed within QPVP since no redox waves from $SiW_{12}O_{40}^{4-}$ occur there. In contrast to cysteamine SAMs serving as positively charged precursor films, SAMs of 3-mercaptopropionic acid is also successfully used to provide negatively charged platforms for first loading cationic polymer QPVP-Os and then anchoring anionic POMs' layers (e.g., Figure 10C). The strategy used here has been successfully popularized to some IPAs as well as other HPAs with different structure and composition, such as Keggin-type $XM_{12}O_{40}^{n-}$ (X = P, Si, Ge; M = W, Mo), Dawson-type $X_2M_{18}O_{62}^{n-}$ (X = P, As; M = Mo, W), and a series of polybasic lanthanide complexes $Ln(SiMo_7W_4O_{39})_2^{13-}$ (Ln = La, Ce, Pr, Nd, Sm, Eu, Gd, Dy, and Yb). More attractive than previous strategies,[4a,18,19] ours is a general one suitable for anchoring nearly all kinds of POMs on Au electrodes covered with alkanethiol SAMs.

4. Concluding Remarks

1. A novel method for film formation first developed by us, the electrochemical growth, has been proven to bear many remarkable advantages over the commonly used immersion growth and is proposed to be widely used in preparing other kinds of composite films.

2. A general modification strategy has been developed for anchoring nearly all kinds of POMs on Au electrodes covered with alkanethiol SAMs based on electrostatic interaction.

3. The thickness, composition, and physicochemical properties of the multilayers can be varied, controlled, and tailored to meet the practical needs at a molecular level.

4. The ease of fabricating multilayer structures from a variety of different POMs makes it possible to prepare complex molecular organizations containing more than one kind of POMs in a multilayer, i.e., forming some heterostructures, which is under active studies in our group.

5. These novel tunable monolayer and multilayer films may find applications as diverse as in electrochromism, photoelectrochemistry, sensors, catalysis, light imaging, and other thin-film molecular devices.

Acknowledgment. This work was supported by the National Science Foundation of China. We are very grateful to Professor Xi Zhang for supplying QPVP-Os.

Supporting Information Available: XPS characterization of S 2p, Mo 3d, N 1s, Os 4f and in BE of 0−70 eV, and FTIR-RA spectra of multilayers at various stages of formation. This material is available free of charge via the Internet at http://pubs.acs.org.

CM9806127